PROCEEDINGS PAPER

X-ray imaging of silicon die within fully packaged semiconductor devices

Brian K. Tanner [ID],[1,2,a)] Patrick J. McNally,[2] and Andreas N. Danilewsky[3]

[1]*Department of Physics, Durham University, Durham DH1 3LE, UK*
[2]*School of Electronic Engineering, Dublin City University, Dublin 9, Ireland*
[3]*Kristallographie, Albert-Ludwigs-Universität Freiburg, Hermann-Herder-Str. 5, D-79104 Freiburg, Germany*

X-ray diffraction imaging (XRDI) (topography) measurements of silicon die warpage within fully packaged commercial quad-flat no-lead devices are described. Using synchrotron radiation, it has been shown that the tilt of the lattice planes in the Analog Devices AD9253 die initially falls, but after 100 °C, it rises again. The twist across the die wafer falls linearly with an increase in temperature. At 200 °C, the tilt varies approximately linearly with position, that is, displacement varies quadratically along the die. The warpage is approximately reversible on cooling, suggesting that it has a simple paraboloidal form prior to encapsulation; the complex tilt and twisting result from the polymer setting process. Feasibility studies are reported, which demonstrate that a divergent beam and quasi-monochromatic radiation from a sealed X-ray tube can be used to perform warpage measurements by XRDI in the laboratory. Existing tools have limitations because of the geometry of the X-ray optics, resulting in applicability only to simple warpage structures. The necessary modifications required for use in situations of complex warpage, for example, in multiple die interconnected packages are specified. © *The Author(s), 2021. Published by Cambridge University Press on behalf of International Centre for Diffraction Data. This is an Open Access article, distributed under the terms of the Creative Commons Attribution licence (http://creativecommons.org/licenses/by/4.0/), which permits unrestricted re-use, distribution, and reproduction in any medium, provided the original work is properly cited.* [doi:10.1017/S088571562100021X]

I. INTRODUCTION

Next-generation advanced integrated circuit technologies will feature "More than Moore" approaches using the heterogeneous integration of semiconductor-based devices, including multiple silicon die. The development of a non-destructive, *in situ* metrology that can analyse the warpage or bow of the semiconductor die inside such devices is particularly challenging. Ideally, such a metrology would be capable of real-time measurement of the die warpage during annealing or curing processes, particularly as a means of pinpointing the impact of crucial process steps. A relatively recent survey (Marks *et al*., 2014) indicated that none of the currently available commercial techniques was capable of *in situ* and non-destructive measurement of the nature and scale of wafer or die bow/warpage across an entire die. For example, profilometry techniques, such as shadow Moiré interferometry (Post *et al*., 2000; Han, 2003), measure only the macroscopic warpage of the complete package, not the chip itself. Furthermore, there is no consensus on the implementation of *in situ* analysis of die warpage when the package is undergoing thermal processing steps or is otherwise at an elevated temperature.

The use of high-resolution X-ray diffraction to measure quantitatively the deflection of encapsulated silicon wafers was reported by Toda and Ikarashi (2010), who were able to separate signals from three stacked chips within a single package. Wong *et al*. (2014) subsequently used such a scanning diffractometry method to show the impact of high temperature on an encapsulated die. Both groups used conventional laboratory X-ray generators. X-ray diffraction imaging (XRDI), originally known as X-ray topography (Bowen and Tanner, 2006), has been used in section geometry to image localized defects in single crystals since its invention by the late (Lang, 1957). Using synchrotron radiation of typically 32 keV, it has been shown that white beam section topography imaging can be used to map quantitatively the warpage in fully packaged silicon die (Bose *et al*., 2016; Cowley *et al*., 2016; Tanner *et al*., 2017).

Despite the success of this technique with the continuous spectrum of white synchrotron radiation, for the technique to have a significant industrial application, it must be transferred for use with a conventional X-ray source and located in fab or, at the very least, in an on-site research laboratory. In this paper, the application of the synchrotron-based technique to the study of the warpage as a function of temperature in a commercial quad-flat no-lead (QFN) chip package is illustrated and the possible use of a divergent beam and characteristic X-ray lines for the warpage measurement of such encapsulated die using a laboratory X-ray source is explored. All synchrotron radiation data presented here were collected at the beamline B16 of the Diamond Light Source, Didcot, UK.

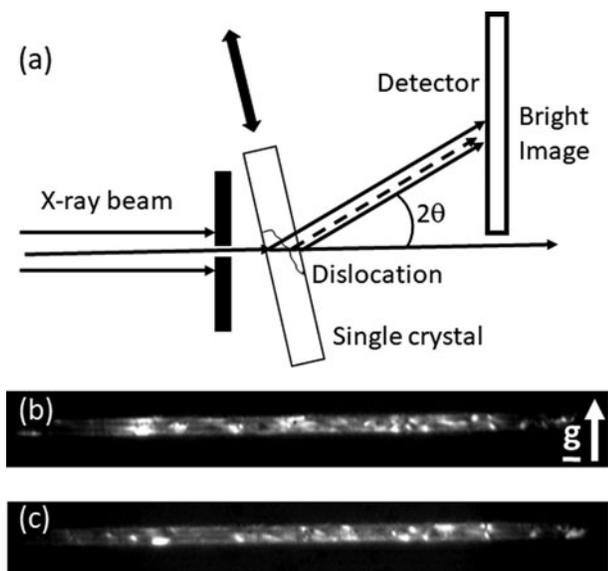a)Author to whom correspondence should be addressed. Electronic mail: b.k.tanner@durham.ac.uk

Figure 1. (a) Schematic diagram of section imaging method. (b) Diffraction image of a (0001) SiC wafer. (c) Image of the displaced wafer: [11$\bar{2}$0] diffraction vector vertical. Image length 2.8 mm. In this geometry, the image height parallel to the diffraction vector is given approximately by $2t\sin\theta_B \; sec2\theta_B$, where t is the crystal thickness and θ_B is the diffraction angle. The image width is determined by the section slit length or crystal size, whichever is smaller.

II. SYNCHROTRON RADIATION METHODOLOGY

The white beam section imaging technique relies on positioning a slit, typically $15 \, \mu m \times 10$ mm, before the sample, which is adjusted such that a narrow ribbon beam is diffracted perpendicular to the extended length [Figure 1(a)]. Defects such as dislocations show as bright regions in the image stripe. For a flat, undistorted wafer, such as the (0001) SiC crystal illustrated in Figures 1(b) and 1(c), when the crystal is translated, different defects, or parts of defects, appear in the image, but the overall image position remains in the same place. There is no displacement of the overall image stripe between Figures 1(b) and 1(c).

However, if the wafer is distorted, as in Figure 2(a), there is a displacement of the image. Although the white synchrotron radiation beam is highly parallel, if the lattice planes are tilted $\delta\theta$ with respect to the original position, the crystal selects a different wavelength from the continuous spectrum to diffract. Because of the different Bragg angle, it immediately follows that the direction of the diffracted beam is changed by $2\delta\theta$ and the image is displaced $2L\delta\theta$, where L is the specimen to detector distance. Thus, by simply measuring the image displacement as a function of specimen position, the angular tilt, that is, the warpage, can be mapped directly. For high X-ray energy, there is little sensitivity to dilation. Provided that the radiation is of sufficiently high energy that
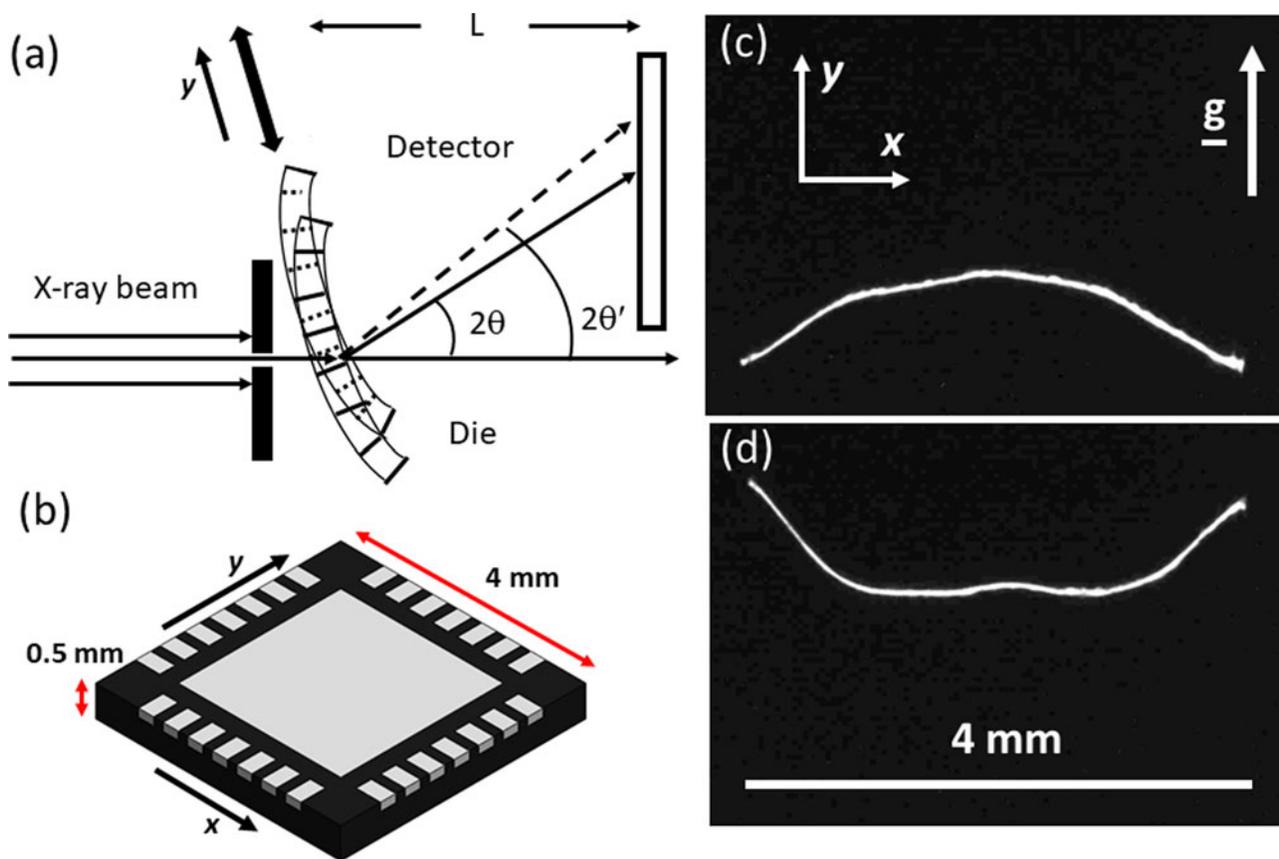

Figure 2. (a) Schematic diagram of change in diffracted beam direction as a curved crystal is scanned. (b) Format and dimensions of uQFN chip packages. (c) Diffraction image from near the bottom of the Si die in an AD9253 QFN package showing twist. (d) Image from sample translated 2.8 mm in the y-direction: 220 reflection and diffracted beam energy 25.8 keV (wavelength 0.48 Å).

the diffracted beam is not totally absorbed, silicon die in fully packaged devices can be examined non-destructively. Packages that can be examined successfully [Figure 2(b)] are the micro QFN (uQFN) format, which is $4 \times 4 \times 0.5$ mm (e.g. PIC16LF1827), and the similar QFN format, which is $7 \times 7 \times 0.75$ mm (e.g. AD9253).

Figures 2(c) and 2(d) show images from the 4.5×4.5 mm Si die in a QFN Analog Devices AD9253 analog-to-digital converter chip. Each image, recorded in transmission on the Photonic Science X-ray MiniFDI camera system with the white beam at beamline B16 at the Diamond Light Source, took about 500 ms to capture. This interval comprised 300 ms exposure and approximately 200 ms specimen displacement time between each position on the sample. Enough data to reconstruct a complete warpage map can be obtained in under a minute.

XRDI images are sensitive to tilt only in the direction of the diffraction vector **g**. It is evident from the shape of the image in Figure 2(c) that there is a twist between the centre and edges of the Si die of $0.20 \pm 0.01°$. Translation of the sample by 2.8 mm results in an overall displacement of the image [Figure 2(d)] and a reversal in the sense of the twist between centre and edges. The tilt between the two translation positions, measured along the line of the die centre, is also $0.2 \pm 0.01°$. The twist now differs between the two edges, being $0.22°$ on the left and $0.18°$ on the right. Absolute accuracy is set primarily by the accuracy of determining the specimen to detector distance; the relative precision of the measurements is about $0.004°$.

A. Change in die warpage during heating of AD9253 chip package

The warpage of the AD9253 die was measured, using the above technique at beamline B16 of the Diamond Light Source, as the sample was heated with a carbon heater, with the temperature being monitored with a thermocouple. As the temperature increased, there was an initial reduction in the angular position at the centre of the die [squares in Figure 3(a)], a reversal of the sign of the change in tilt occurring at 100 °C in both of the samples measured. Upon an increase in temperature to 150 °C, the tilt reverted to that at room temperature and at 200 °C, and the tilt further increased. Cooling the sample reversed the process, the angular position again going through a minimum and the final room temperature value being displaced, but by only $0.025 \pm 0.006°$, from the initial starting value. Across the centre of the die, the twist was almost zero in both samples, and this changed little as a function of temperature [Figure 3(a)]. At the bottom of the sample ($y = 0$), the tilt at the centre and at the edges (in the x-direction) showed a similar U-shaped variation with temperature. The twist between edge and centre, however, fell as the temperature increased, this variation being approximately linear with temperature when above 50 °C [Figure 3(b)]. Finally, it is noted that, although the tilt at the centre point in the x-direction ($x = 2.2$ mm) as a function of y-position did not exhibit a monotonic variation at room temperature [Figure 3(c)], at high temperature, the tilt became almost linear with temperature. During manufacture, the device is set in the polymer potting compound of the package at an elevated temperature, of the order of 150 °C. As the polymer cools and becomes solid, the strain in the sample becomes complex,
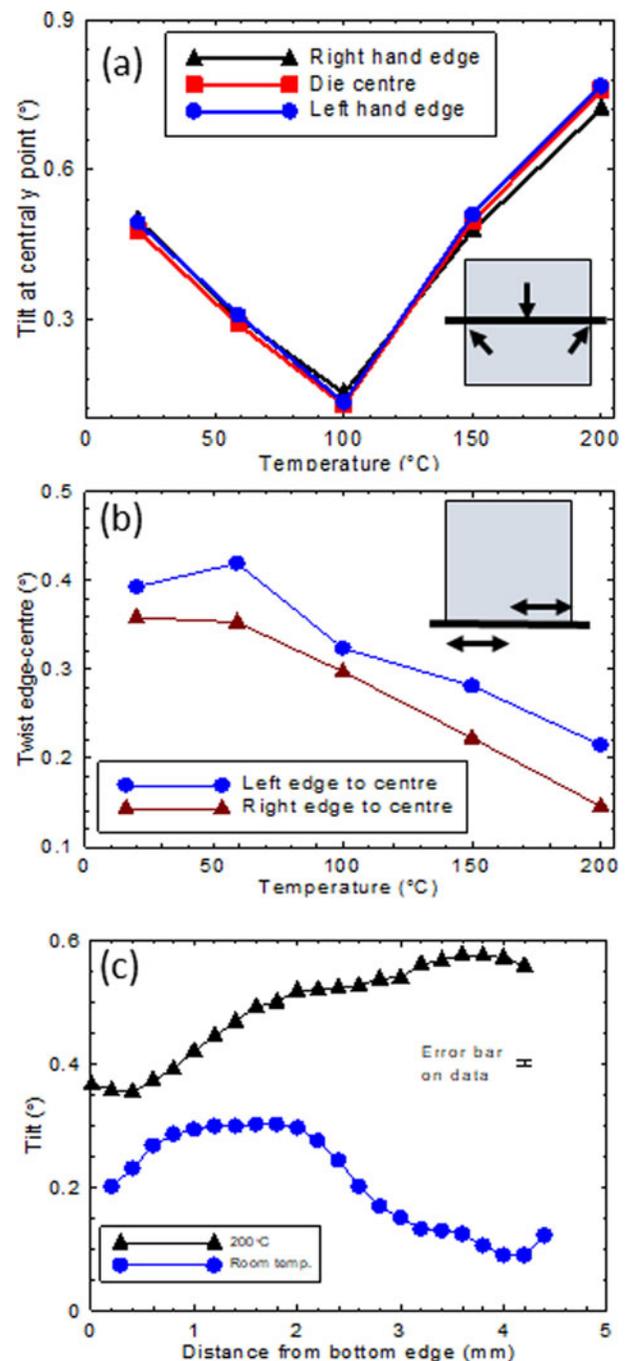

Figure 3. (a) Variation of the relative tilt at points along the central line of the die as a function of temperature. (b) Variation in twist across the bottom edge of the die as a function of temperature. (c) Relative tilt along die x-position centre line as a function of y-position for 200 °C and room temperature. Error in the precision of individual data points is less than the data mark size.

resulting in the non-symmetric tilt and twist behaviour at room temperature. When the temperature is subsequently raised, the polymer reverts to its high-temperature viscous state and the die relaxes back to the simple linear tilt pattern associated with gluing to the lead frame.

While the precision of the measurement of change in tilt is very high for the synchrotron radiation section topography method, the variation in distortion between the AD9253 chips studied was considerable. This contrasted with packages that showed simple paraboloidal warpage, such as the
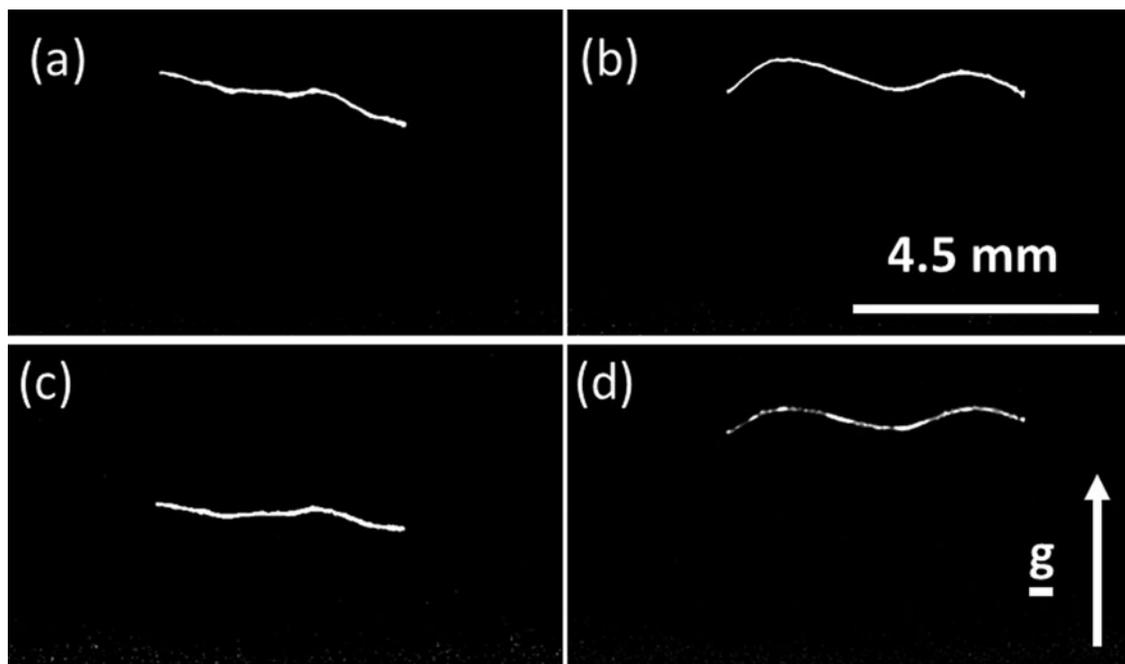
Figure 4. Section topographs through the centre of the die for two AD9253 packages: (a) Chip 1 at 20 °C, (b) Chip 2 at 20 °C, (c) Chip 1 at 150 °C, and (d) Chip 2 at 150 °C.

PIC16LF1827 devices discussed below, which were much more reproducible (see also Tanner *et al.*, 2017). An example is shown in Figure 4 of the tilt and twist differences across the centres of two AD9253 chips at room temperature and at 150 °C. At room temperature in the as-received state, there is significant difference in the twist across the die, indicated by
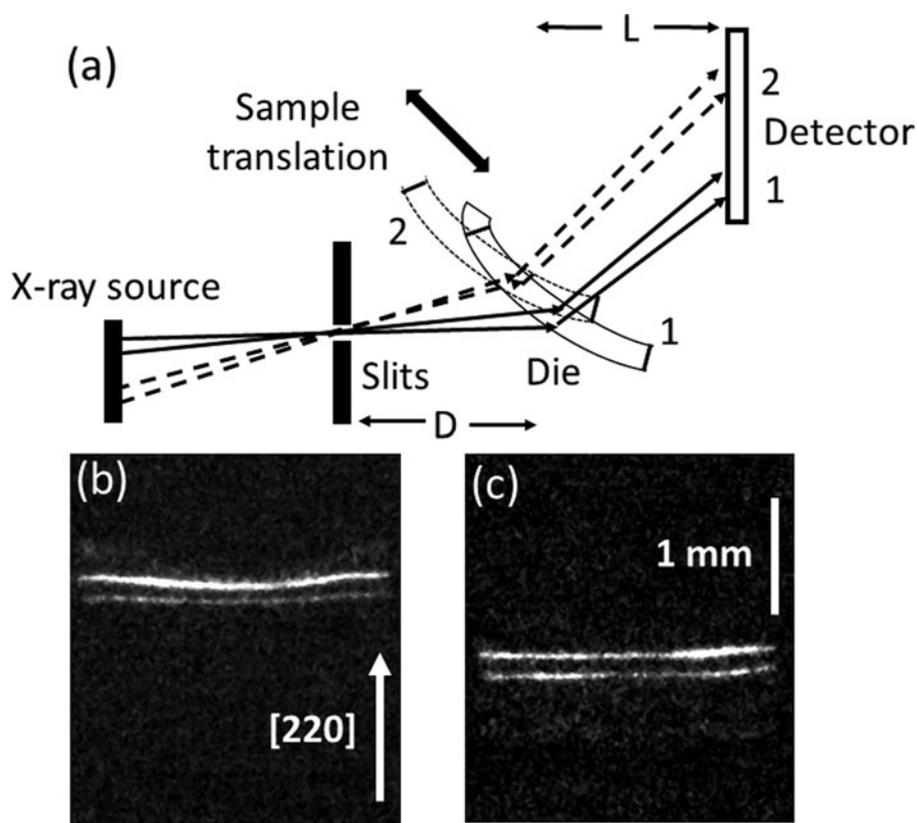

Figure 5. (a) Schematic diagram, rotated by 90° from the actual tool orientation for consistency, of the divergent beam geometry within the Bruker tools. (b) Images of the characteristic $AgK\alpha_1$ and $AgK\alpha_2$ lines from the Si die in a Microchip PIC16LF1827 microcontroller of the total uQFN package dimension $4 \times 4 \times 0.5$ mm. (c) Displacement of lines on translation by 0.75 mm: 220 reflection. Each image took 10 s to capture. The height of the die in the horizontal dimension is magnified by 1.4 because of the projection geometry parallel to the diffracting planes. Data collected on a Bruker JVSensus XRDI tool.
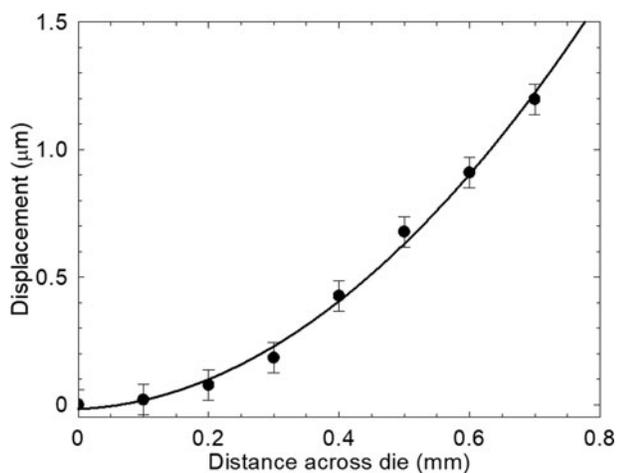
Figure 6. Absolute displacement of the surface of the silicon die shown in Figure 5 with respect to the *y*-position across the die. The solid line is a quadratic fit to the data.

the different lateral shape of the images. For Chip 1, there was an approximately linear change in twist across the device, whereas Chip 2 showed a bimodal profile, with the twist between the two die edges being almost zero. Upon heating

to 150 °C, Chip 1 showed a considerable change in tilt, indicated by the displacement of the whole image, and a reduction in twist, shown by the lower gradient of the line across the page. In contrast, Chip 2 exhibited an almost identical tilt and twist at 150 °C to that at room temperature. There was, however, a similar reversal of overall tilt change upon heating of the two chips, equivalent to Figure 3(a). Presently, it is not possible to provide further statistics on the range of this variability.

III. DIVERGENT BEAM FROM A LABORATORY SOURCE

The X-rays emitted from laboratory X-ray tubes differ from synchrotron radiation, in that they are emitted into 2π solid angles, and although the X-ray spectrum does contain a continuous range of wavelengths in the Bremsstrahlung, the most intense features are the characteristic lines of the element(s) in the source-target material. Thus, exploiting the divergence of the beam and one of the characteristic lines in a quasi-monochromatic mode would seem a promising approach to devising a rapid laboratory technique for warpage measurement. The use of a silver target X-ray tube provides
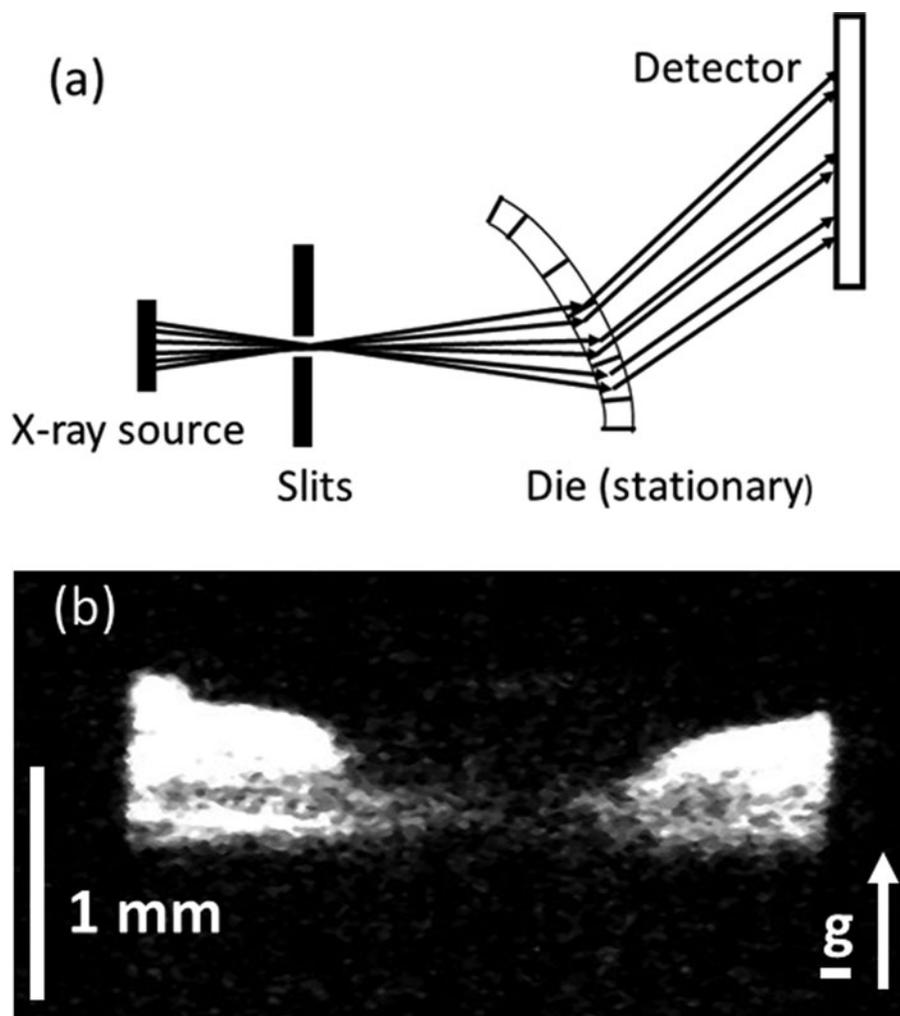

Figure 7. (a) Schematic diagram of simultaneous diffraction across the convex silicon crystal of the characteristic Ag$K\alpha$ lines. (b) The resulting broad image formed by simultaneous diffraction and from the overlap of the characteristic lines. PIC16LF1827 chip exit and entrance surfaces reversed from Figure 5. The Bruker JVSensus tool used in standard configuration: 220 reflection.

closely spaced characteristic Ag$K\alpha_1$ and Ag$K\alpha_2$ lines at 22.16 keV (0.5594 Å) and 21.99 keV (0.5638 Å), respectively, or the $K\beta_1\beta_3$ unresolved doublet of average energy 24.94 keV at 25% of the $K\alpha_1$ intensity. All are transmitted with modest attenuation through the uFQN package thickness of 500 μm.

The Bruker JVSensus and JVQC-TT XRDI tools can be equipped with a silver X-ray tube, and although optimized for the study of strains, including those from dislocations, by X-ray topography in single crystals of semiconductors (Atrash *et al.*, 2017), they have a beam divergence that makes them appropriate for feasibility studies. The tools are based on the BedeScan concept originally developed by Bowen *et al.* (2003) and were initially operated in their standard geometry, with a 200 μm (adjustable) slit located midway between the source and the sample. The geometry is shown in Figure 5(a), with the sample to detector distance L being variable. With such a divergent beam, at the detector, one effectively observes the spectrum from the X-ray tube spread out in space. When set at the appropriate angle, the $K\alpha_1$ and $K\alpha_2$ characteristic lines are observed [Figure 5(b)], the line width being set by the fundamental linewidth of the atomic transition, convolved with the slit function. For an undistorted wafer, straight lines result, which do not change position as the wafer is translated across the beam for a fixed position of the detector. When the wafer is warped, characteristic X-rays from a different point on the X-ray tube target can satisfy the Bragg angle at an absolute angle that differs by the wafer tilt. Because these beams of characteristic radiation travel in different directions to that in the undistorted wafer, and there is no slit between wafer and detector, the characteristic lines are displaced by $(L + D)\delta\theta$ because of the tilt $\delta\theta$ as the warped wafer is scanned across the slit [Figure 5(c)]. Here, D is the distance between slits and sample. Note that for the PIC16LF1827 microcontroller illustrated below, there is little twist across the die. Radiographs showed the die to be a square of side 2.1 mm.

The beam divergence in the diffracting plane is 0.2° for the standard JVSensus geometry, so this sets a limit to the angular range of warpage that can be measured. Furthermore, in the standard geometry [Figure 5(a)], with respect to the narrow slits, the position on the die at which the diffraction occurs changes as the warped sample is translated. There is, therefore, no simple correspondence between the change in position on the detector and the warpage angle. This problem can be minimized by locating the slit close to the sample, and the data shown in Figure 5 were collected on a Bruker JVQC-TT XRDI tool with a 200 μm wide slit located about 10 mm from the sample. However, this also reduced the divergence, and hence the range of tilt sampled, to 0.11°. If the warpage is uniform, that is the change in angle is linear with distance along the die, it is possible to correct for the geometric shift analytically.

Unlike the QFN AD9253 chip, the image displacement from the uQFN format Microchip PIC16LF1827 microcontroller was found to be linear with translation, and when the small correction is made for the change in sampling position, the gradient k of the true tilt as a function of distance was determined to be $0.30 \pm 0.02°$ mm^{-1}, consistent with that found at the synchrotron radiation source. The absolute displacement Δz of the die is related to the incremental change in angular displacement $d\theta$ with distance increment dy in the
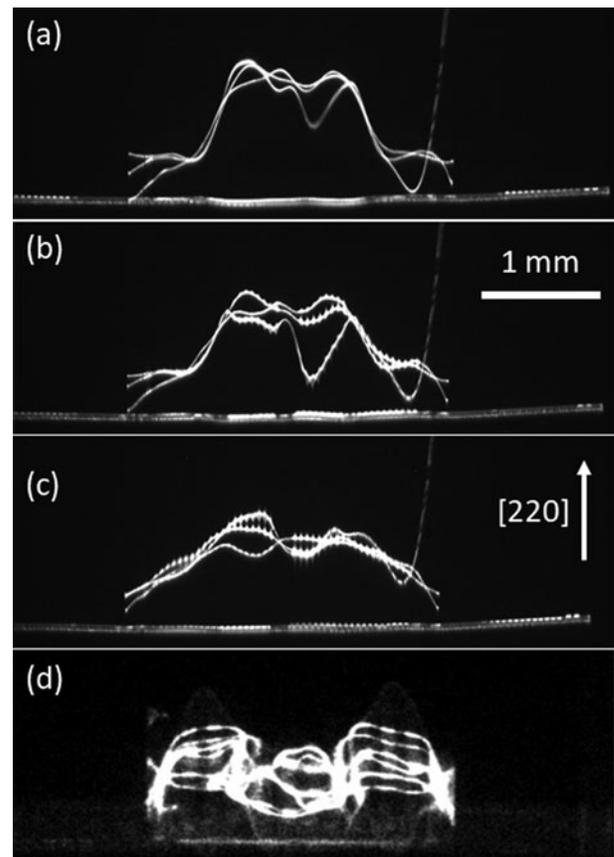

Figure 8. Images of interconnected four-die stacks of three thin (50 μm) and one thick (200 μm) die. (a)–(c) show images taken at B16 of the diamond light source, there being a translation of the die of 0.06 mm in the y-direction between each image. (d) Typical image with divergent beam and Ag$K\alpha_1$ and $K\alpha_2$ characteristic lines. Data taken on a Bruker JVQC-TT tool: 220 reflections.

surface by

$$\Delta z = \int y d\theta = \int k y dy = \frac{ky^2}{2} \qquad (1)$$

This parabolic displacement (Figure 6), which is found in both of the two orthogonal directions in the plane of the die, is characteristic of the warpage when a small die is fixed to the lead frame with glue at each of the four corners and would suggest that the distortion of the small die by the encapsulation polymer is less than that of the larger silicon pieces in the QFN packages.

The geometry of Figure 5 has a further important limitation. Warpage can be measured accurately only when, viewed from the detector, the curvature of the die is concave, as illustrated in Figure 5. If the warpage is convex, as illustrated in Figure 7(a), the silicon die becomes effectively a curved crystal focusing monochromator. From any point on the source, the convex curvature of the silicon die crystal enables the diffraction angle for the characteristic lines to be simultaneously satisfied across a range of positions on the crystal. This effect is most pronounced when the Bruker tools are used in standard geometry. As shown in Figure 7(b), the image is then not a pair of sharp lines, but a blurred and wide image. For small warpage, this can be partially rectified by locating the slit

close to the sample. For the PIC16LF1827 chip shown in Figure 5, with the slit 10 mm being from the sample, the broadening was reduced to approximately the separation of the $K\alpha_1$ and $K\alpha_2$ lines.

For simple warpage, such as in the PIC16LF1827 chip, by maintaining the orientation of the device to be concave with respect to the X-ray exit beams, sharp lines can readily be obtained, and high-resolution warpage mapping achieved with the divergent beam geometry. However, in the case of four-die stacks fabricated for the authors at IMEC in Leuven, Belgium, the curvature is much more complex. These unencapsulated devices consist of an interconnected four-die stack, the three top dies being 5 mm × 5 mm × 50 μm thick, while the bottom die is 8 mm × 8 mm × 200 μm thick. With the white beam synchrotron radiation section topography technique [Figures 8(a)–8(c)], there are four very clearly separated images from the individual dies, with the thick bottom die being almost undistorted, while the top three thin dies are very strongly warped by the interconnect and die adhesion processes. Despite the high resolution of the images, it is difficult to track the tilt as a function of position of the individual thin die when the curvature changes rapidly from convex to concave over quite a small die displacement and where there is also substantial twist, such as illustrated in Figure 8. With the divergent beam technique, it becomes even more difficult to follow the individual die images [Figure 8(d)]. The broadening of the image as the curvature becomes convex with respect to the detector brings all the individual images together. Although there are two clear α_1 and α_2 images from each die when the curvature is concave, this is not the case when it becomes convex.

IV. CONCLUSION

The effectiveness of XRDI for the examination and measurement of the warpage of die in fully packaged chips at synchrotron radiation sources is now fully established. Restrictions on the type of package capable of being examined are primarily set by the X-ray energy (wavelength) limit of the bending magnet or insertion devices used. It has been shown that for a standard bending magnet such as at B16 of the Diamond Light Source, QFN and uQFN format chips can be studied satisfactorily. When one such chip, the AD9253, was raised in temperature to 200 °C, the curvature of the 4.5 × 4.5 mm die simplified, resulting in an approximately constant gradient of tilt with respect to position across the die surface. This, together with a reduction in twist across the die and approximate reproducibility of the warpage on subsequent cooling, suggests that the curvature from gluing the sample was of simple paraboloidal form prior to the polymer encapsulant being applied. As this cooled and hardened, the strains became more non-uniform.

The divergent beam quasi-monochromatic method, when used with a silver anode X-ray tube, appears to have the potential for such studies in the laboratory or fab. While the Bruker JVSensus and JVQC-TT XRDI tools, to which the authors were kindly granted access, are optimized for imaging strains and thus are not totally appropriate for warpage measurement in their standard configuration, they do amply demonstrate the feasibility of the method. Key limitations of the current tools are a limited divergence, and because of the separation of slit from sample, there is a broadening of the characteristic line images when the die is convex with respect to the detector. For a commercial inspection tool, this blurring could be minimized by restriction to a single Bragg angle and having the slit assembly surface oriented parallel to the sample, thus enabling scanning with a very small slit-sample distance.

Atrash, F., Meshi, I., Krokhmal, A., Ryan, P., Wormington, M., and Sherman, D. (**2017**). "Crystalline damage in silicon wafers and 'rare event' failure introduced by low-energy mechanical impact," Mater. Sci. Semicond. Process. **63**, 40–44.

Bose, A., Vijayaraghavan, R. K., Cowley, A., Cherman, V., Tanner, B. K., Danilewsky, A. N., De Wolf, I., and McNally, P. J. (**2016**). "Nondestructive monitoring of die warpage in encapsulated chip packages," IEEE Trans. Compon. Packaging Manuf. Technol. **6**, 653–662.

Bowen, D. K. and Tanner, B. K. (**2006**). *X-ray Metrology in Semiconductor Manufacturing* (CRC Taylor and Francis, Boca Raton).

Bowen, D. K., Wormington, M., and Feichtinger, P. (**2003**). "A novel digital X-ray topography system," J. Phys. D: Appl. Phys. **36**, A17–A23.

Cowley, A., Ivankovic, A., Wong, C. S., Bennett, N. S., Danilewsky, A. N., Gonzalez, M., Cherman, V., Vandervelde, B., De Wolf, I., and McNally, P. J. (**2016**). "B-spline X-ray diffraction imaging – rapid nondestructive measurement of die warpage in ball grid array packages," Microelectron. Reliab. **59**, 108–116.

Han, B. (**2003**). "Thermal stresses in microelectronics subassemblies: quantitative characterization using photomechanics method," J. Thermal Stresses **26**, 583–613.

Lang, A. R. (**1957**). "A method for the examination of crystal sections using penetrating characteristic X radiation," Acta Metall. **5**, 358–364.

Marks, M. R., Hassan, Z., and Cheong, K. Y. (**2014**). "Characterization methods for ultrathin wafer and die quality: a review," IEEE Trans. Compon. Packaging Manuf. Technol. **4**, 2042–2057.

Post, D., Han, B. T., and Ifju, P. G. (**2000**). "Moire methods for engineering and science – Moire interferometry and shadow Moire," Top. Appl. Phys. **77**, 151–196.

Tanner, B. K., Danilewsky, A. N., Vijayaraghavan, R. K., Cowley, A., and McNally, P. J. (**2017**). "Non-destructive X-ray diffraction measurement of warpage in silicon die embedded in integrated circuit packages," J. Appl. Crystallogr. **50**, 547–554.

Toda, A. and Ikarashi, N. (**2010**). "Nondestructive Warpage measurements of LSI chips in a stacked system in package by using high-energy X-ray diffraction," Jpn. J. Appl. Phys. **49**, 04DB03.

Wong, C. S., Bennett, N. S., Manessis, D., Danilewsky, A., and McNally, P. J. (**2014**). "Non-destructive laboratory-based X-ray diffraction mapping of warpage in Si die embedded in IC packages," Microelectron. Eng. **117**, 48–56.